



Orange red iridium complexes with good electron mobility and mild OLED efficiency roll-off

Yong-Hui Zhou ^{a,1}, Dong Jiang ^{b,1}, You-Xuan Zheng ^{c,*}

^a Jiangsu Key Laboratory of Atmospheric Environment Monitoring and Pollution Control, Collaborative Innovation Center for Atmospheric Environment and Equipment Technology, College of Environmental Science and Engineering, Nanjing University of Information Science & Technology, Nanjing, 210044, PR China

^b School of Chemistry and Pharmaceutical Engineering, Taishan Medical University, Tai'an, 271016, PR China

^c State Key Laboratory of Coordination Chemistry, Collaborative Innovation Center of Advanced Microstructures, Jiangsu Key Laboratory of Advanced Organic Materials, Nanjing National Laboratory of Microstructures, School of Chemistry and Chemical Engineering, Nanjing University, Nanjing, 210093, PR China

ARTICLE INFO

Article history:

Received 16 June 2018

Received in revised form

2 September 2018

Accepted 17 September 2018

Available online 19 September 2018

Keywords:

OLED

Orange red iridium complexes

1,3,4-Oxadiazole derivative

1,3,4-Thiadiazol derivative

Electron mobility

ABSTRACT

Two iridium(III) complexes with 1-(3,5-bis(trifluoromethyl)-pyridin-4-yl)isoquinoline (**tntpiq**) as main ligand, 2-(5-pyridin-4-yl)-1,3,4-oxadiazol-2-ylphenol (**pop**) and 2-(5-pyridin-4-yl)-1,3,4-thiadiazol-2-ylphenol (**psp**) as ancillary ligands were investigated. Both complexes emit orange red lights with different photoluminescence efficiencies (**Ir(tntpiq)₂(pop)**: $\lambda_{\text{em}} = 585 \text{ nm}$, $\Phi = 0.41$ and **Ir(tntpiq)₂(psp)**: $\lambda_{\text{em}} = 590 \text{ nm}$, $\Phi = 0.59$). Moreover, the electron mobility values of the two complexes are higher than that of the electron transport material Alq₃ (tris(8-hydroxyquinoline)aluminium), which are beneficial for their performances in organic light-emitting diodes (OLEDs). The devices with a structure of ITO/MoO₃ (3 nm)/TAPC (1,1-bis[4-[N,N-di(p-tolyl)amino]pyridin-4-yl]cyclohexane, 30 nm)/Ir(III) complexes (2 wt%): 26DCzPPy (2,6-bis(3-(carbazol-9-yl)pyridin-4-yl)pyridine, 10 nm)/TmPyPB (1,3,5-tri(*m*-pyrid-3-yl)pyridin-4-yl)benzene, 40 nm)/LiF (1 nm)/Al (100 nm) displayed similar performances with a maximum current efficiency of 24.3 cd A⁻¹ and a maximum external quantum efficiency of 11.6%, respectively, and the efficiency roll-off is very mild.

© 2018 Elsevier B.V. All rights reserved.

1. Introduction

Organic light emitting diodes (OLEDs) have received great attention because of their successful applications in flat-panel displays and solid-state lighting. Cyclometalated iridium(III) complexes are almost the most promising phosphorescent guest materials for highly efficient OLEDs due to their lifetime on the microsecond time-scale, high quantum yields, flexibility in color tuning and excellent thermal stability [1–28]. Furthermore, the phosphorescence of Ir(III) complexes generates by the metal-to-ligand charge transfers (MLCT) and ligand-centered (LC) transition [29], so that it is possible to control the excited state's energy level by adjusting ligands via the substituent effect.

It is well-known that the balance of the electron-hole injection and transport is necessary for high efficient OLEDs using the Ir(III)

complexes because both the charge carrier balance deterioration and nonradioactive quenching processes increase will cause a serious efficiency roll-off. Since the majority of hole-transporting materials' hole mobility is much higher than the electron-transporting materials' electron mobility, the OLEDs performances depend on electron transport's capability. Therefore, the use of ambipolar host materials is essential to gain phosphorescent OLEDs with low efficiency roll-off, as well as the synthesis of dopants with excellent electron mobility.

From former work, the bulky trifluoromethyl ($-\text{CF}_3$) substituents can affect the molecular packing and the steric protection surrounding the metal would restrain the self-quenching impact, and the C–F bond with low vibrational frequency can reduce radiationless deactivation rate [30–33]. Besides that, nitrogen heterocycle would also enhance the electron affinity and the electron mobility of the Ir(III) complexes. Therefore, the Ir(III) complexes with main ligands containing 2,6-bis(trifluoromethyl) pyridin unit always show good device performances [34–37]. Moreover, OLEDs based on Ir(III) complexes with 1,3,4-oxadiazole

* Corresponding author.

E-mail address: yxzheng@nju.edu.cn (Y.-X. Zheng).

¹ Zhou and Jiang have same contributions to this paper.

derivatives as ancillary ligands also have good performances due to their high electron mobility, high photoluminescence quantum yield and good thermal, chemical stability [38–40], which would enhance the electron affinity and the electron mobility of the Ir(III) complexes.

On this basis, as shown in **Scheme 1**, two heteroleptic Ir(III) complexes (**Ir(tntpiq)₂(pop)** and **Ir(tntpiq)₂(psp)**) were prepared with 1-(3,5-bis(trifluoromethyl)pyridin-4-yl)isoquinoline (tntpiq) as main ligand, 2-(5-pyridin-4-yl)-1,3,4-oxadiazol-2-ylphenol (pop) and 2-(5-pyridin-4-yl)-1,3,4-thiadiazol-2-ylphenol (psp) as ancillary ligands. These complexes containing 2,6-bis(trifluoromethyl)pyridin unit and 1,3,4-oxadiazole/1,3,4-thiadiazole derivatives would have good electron mobility and high photoluminescence quantum yield. Therefore, the devices based on two emitters displayed good performances with a maximum external quantum efficiency up to 11.6% and very low efficiency roll-off.

2. Experimental section

2.1. General information

¹H NMR spectra were measured on a Bruker AM 500 spectrometer. Electrospray ionization mass spectra (ESI-MS) were obtained with ESI-MS (LCQ Fleet, Thermo Fisher Scientific) and Matrix Assisted Laser Desorption Ionization Time of Flight Mass Spectrometry (autoflex TOF/TOF, Bruker Daltonics). Elemental analyses for C, H and N were performed on an Elementar Vario MICRO analyzer. TGA measurements were carried out on a DSC 823e analyzer (METTLER). UV-vis absorption and photoluminescence spectra were measured on a Shimadzu UV-3100 and a Hitachi F-4600 spectrophotometer at room temperature, respectively. A conventional three-electrode configuration, consisting of Glassy Carbon Electrode (GCE) as working electrode, a Pt wire counter electrode, and a reference electrode of Ag/AgNO₃ (0.1 M), was used to record cyclic voltammetry data in nitrogen-deaerated CH₃CN solution with 0.1 M [Bu₄N]ClO₄ as the supporting electrolyte and

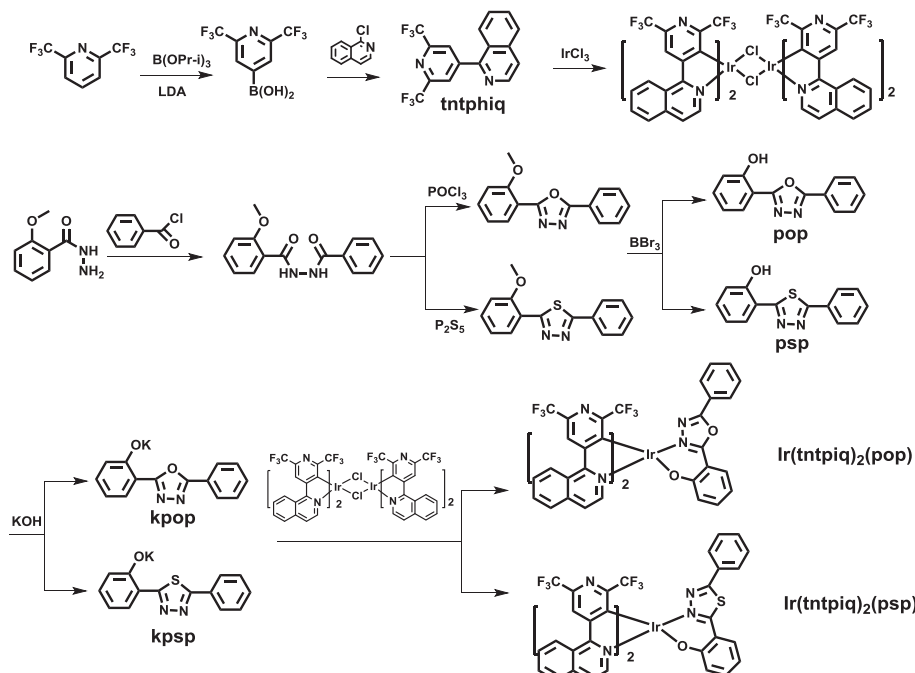
ferrocene as internal standard at a scan rate of 50 mV/s.

2.2. X-ray crystallography

X-ray crystallographic measurements of the single crystals were carried out on a Bruker SMART CCD diffractometer (Bruker Daltonics Inc.) using monochromated Mo K α radiation ($\lambda = 0.71073 \text{ \AA}$) at room temperature. Cell parameters were retrieved using SMART software and refined using SAINT [41] program in order to reduce the highly redundant data sets. Data were collected using a narrow-frame method with scan width of 0.30° in ω and an exposure time of 5 s per frame. Absorption corrections were applied using SADABS [42] supplied by Bruker. The structures were solved by Patterson methods and refined by full-matrix least-squares on R^2 using the program SHELXS-2014 [43]. The positions of metal atoms and their first coordination spheres were located from direct-methods E-maps, other non-hydrogen atoms were found in alternating difference Fourier syntheses and least-squares refinement cycles and during the final cycles refined anisotropically. Hydrogen atoms were placed in calculated position and refined as riding atoms with a uniform value of U_{iso} .

2.3. OLEDs fabrication and measurement

All OLEDs were fabricated on the pre-patterned ITO-coated glass substrate with a sheet resistance of 15 Ω sq⁻¹. The deposition rate for organic compounds is 1–2 Å s⁻¹. The phosphor and host were co-evaporated from two separate sources. The cathode consisting of LiF/Al was deposited by evaporation of LiF with a deposition rate of 0.1 Å s⁻¹ and then by evaporation of Al metal with a rate of 3 Å s⁻¹. The effective area of the emitting diode is 0.1 cm². The characteristics of the devices were measured with a computer controlled KEITHLEY 2400 source meter with a calibrated silicon diode in air without device encapsulation. On the basis of the uncorrected PL and EL spectra, the CIE coordinates were calculated using a test program of the spectra scan PR650 spectrophotometer.



Scheme 1. Synthetic routes of the ligand and the complexes.

2.4. Syntheses

All the reagents were used with commercial grade. The ligands and complexes were synthesized under nitrogen atmosphere and the synthetic routes were listed in **Scheme 1**.

2.4.1. Synthesis of tntpiq ligand

A stirred solution of 2,6-bis-(trifluoromethyl)pyridine (0.22 g, 10 mmol) in diethyl ether (20 mL) was cooled to -78°C . LDA (lithium diisopropylamide, 6.0 mL, 10 mmol) was added over 20 min and stirred for 1 h, and then $\text{B}(\text{OPr-i})_3$ (2.89 mL, 12.4 mmol) was injected. The mixture was warmed to room temperature and stirred for another 1 h. The pH was adjusted to 10 by the slow addition of 10% aqueous NaOH solution (20 mL). After 1 h, the organic phase was acidified to $\text{pH} = 4$ by the dropwise addition of 3 N HCl. The extraction with ethyl acetate and evaporation of the organic phase gave the crude corresponding aryl boronic acids. 1-Chloroisoquinoline and 1,1'-bis(diphenylphosphion)ferrocene palladium(II) dichloride (0.3 mmol) and the boronic acids were added in 50 mL THF. After 20 mL of aqueous 2 N K_2CO_3 was delivered, the reaction mixture was heated at 70°C for 1 day. The mixture was poured into water and extracted with CH_2Cl_2 (10 mL \times 3 times). Finally, silica column purification (PE: EA = 10: 1) gave the 1-(2,6-bis(trifluoromethyl)pyridin-4-yl)isoquinoline in 40% yield. ^1H NMR (400 MHz, CDCl_3) δ 8.69 (d, $J = 5.6$ Hz, 1H), 8.26 (s, 2H), 8.00 (d, $J = 8.3$ Hz, 1H), 7.94 (dd, $J = 8.5, 0.8$ Hz, 1H), 7.81 (ddd, $J = 8.2, 5.9, 1.2$ Hz, 2H), 7.69 (ddd, $J = 8.3, 6.9, 1.2$ Hz, 1H). MS(ESI) m/z calcd for $\text{C}_{16}\text{H}_8\text{F}_6\text{N}_2^+$: 352.06 [M] $^+$, found: 353.06 [M+H] $^+$.

2.4.2. General syntheses of iridium complexes

A mixture of IrCl_3 (1 mmol) and tntpiq (2.5 mmol) in 2-ethoxyethanol and water (20 mL, 3:1, v/v) was refluxed for 24 h. After cooling, the solid precipitate was filtered to give the crude cyclometalated Ir(III) chloro-bridged dimer. Then, the slurry of crude chloro-bridged dimer (0.2 mmol) and 2-(5-pyridin-4-yl)-1,3,4-oxadiazol-2-yl)phenol or 2-(5-pyridin-4-yl)-1,3,4-thiadiazol-2-yl)phenol potassium salt (0.5 mmol) in 2-ethoxyethanol (20 mL) was refluxed for 24 h. The solvent was evaporated at low pressure and the mixture was poured into water and extracted with CH_2Cl_2 (10 mL \times 3 times), and then chromatographed to give complexes $\text{Ir}(\text{tntpiq})_2(\text{pop})$ and $\text{Ir}(\text{tntpiq})_2(\text{psp})$, which were further purified by sublimation in vacuum.

Ir(tntpiq)₂(pop). 72% yield. ^1H NMR (400 MHz, CDCl_3) δ 8.84 (dd, $J = 8.3, 4.9$ Hz, 2H), 8.63 (d, $J = 6.5$ Hz, 1H), 8.57 (d, $J = 11.9$ Hz, 2H), 7.94–7.89 (m, 1H), 7.88–7.74 (m, 6H), 7.72–7.66 (m, 2H), 7.55–7.39 (m, 5H), 7.23 (d, $J = 6.5$ Hz, 1H), 6.95 (ddd, $J = 8.7, 6.9, 1.8$ Hz, 1H), 6.45 (d, $J = 8.1$ Hz, 1H), 6.42–6.34 (m, 1H). MS(ESI) m/z calcd for $\text{C}_{46}\text{H}_{23}\text{F}_{12}\text{IrN}_6\text{O}_2$: 1111.93 [M] $^+$, found 1113.01 [M+H] $^+$. MALDI-TOF, m/z : calcd for $\text{C}_{46}\text{H}_{23}\text{F}_{12}\text{IrN}_6\text{O}_2$, 1111.928 [M], found 1111.880 [M]. Anal. Calcd. For $\text{C}_{46}\text{H}_{23}\text{F}_{12}\text{IrN}_6\text{O}_2$: C 49.69, H 2.09, N 7.56. Found: C 49.41, H 2.31, N 7.45.

Ir(tntpiq)₂(psp). 81% yield. ^1H NMR (400 MHz, CDCl_3) δ 8.83 (t, $J = 7.8$ Hz, 2H), 8.72 (d, $J = 6.5$ Hz, 1H), 8.58 (d, $J = 10.1$ Hz, 2H), 7.96–7.87 (m, 1H), 7.88–7.67 (m, 6H), 7.47 (d, $J = 6.5$ Hz, 1H), 7.46–7.40 (m, 1H), 7.40–7.31 (m, 4H), 7.18 (d, $J = 6.5$ Hz, 1H), 7.08 (dd, $J = 8.0, 1.6$ Hz, 1H), 6.83 (ddd, $J = 8.6, 6.9, 1.7$ Hz, 1H), 6.39 (dd, $J = 8.6, 0.9$ Hz, 1H), 6.33–6.27 (m, 1H). MS(ESI) m/z calcd for $\text{C}_{46}\text{H}_{23}\text{F}_{12}\text{IrN}_6\text{OS}$: 1127.99 [M] $^+$, found 1129.17 [M+H] $^+$. MALDI-TOF, m/z : calcd for $\text{C}_{46}\text{H}_{23}\text{F}_{12}\text{IrN}_6\text{OS}$, 1127.989 [M], found 1129.083 [M]. Anal. Calcd. For $\text{C}_{46}\text{H}_{23}\text{F}_{12}\text{IrN}_6\text{OS}$: C 48.98, H 2.06, N 7.45. Found: C 48.86, H 2.37, N 7.31.

3. Results and discussion

3.1. Synthesis and characterization

Scheme 1 shows the chemical structures and synthetic routes of the ligands and Ir(III) complexes. The ligand (tntpiq) was synthesized using a Suzuki coupling reaction. The 2-(5-pyridin-4-yl)-1,3,4-oxadiazol-2-yl)phenol (pop) and 2-(5-pyridin-4-yl)-1,3,4-thiadiazol-2-yl) phenol (psp) ancillary ligands and their potassium salts were prepared according to our previous publications [40,44–46]. The Ir(III) complexes were obtained in two steps with popular methods via Ir(III) chloro-bridged dimer. Purification of the mixture by silica gel chromatography provided crude products, which were further purified by vacuum sublimation. Both compounds were characterized by ^1H NMR, the electrospray ionization mass spectra (ESI-MS) and the elemental analyses for C, H, and N.

Furthermore, the molecular structures of $\text{Ir}(\text{tntpiq})_2(\text{pop})$ and $\text{Ir}(\text{tntpiq})_2(\text{psp})$ complexes were also proved via the single crystals and their crystal diagrams are displayed in **Fig. 1**. The molecular parameters and atomic coordinates are collected in **Table S1**, **Table S2** (Supporting Information), respectively. From the structure diagrams of crystals it can be found that the iridium atom is embraced by C, N and O atoms from tntpiq or pop/psp, with twisted octahedral coordination geometry. For $\text{Ir}(\text{tntpiq})_2(\text{pop})$ and $\text{Ir}(\text{tntpiq})_2(\text{psp})$, angles of [N–Ir–O] are $85.8(2)^{\circ}$ – $86.8(3)^{\circ}$, and the angles of [C–Ir–N] are $79.4(4)^{\circ}$ – $80.9(3)^{\circ}$, respectively. The lengths of Ir–C bonds range from 2.020(8) to 2.041(10) Å. The Ir–N and Ir–O bonds have the lengths of 2.010(9)–2.088(8) Å and 2.087(6)–2.098(7) Å, respectively. These results are similar to the parameters of the cyclometalated Ir(III) complexes that have been reported.

The thermal stability of the material is crucial for efficient and stable OLEDs. If a complex can be applied in practical OLEDs, the decomposition temperature (T_d) and the melting points (T_m) needs to be high enough to guarantee that the complex could be deposited onto the solid face without any decomposition on sublimation. From the thermogravimetric analysis (TGA, **Fig. 2(a)**) curves of $\text{Ir}(\text{tntpiq})_2(\text{pop})$ and $\text{Ir}(\text{tntpiq})_2(\text{psp})$ it is can be figured out that the decomposition temperatures (5% loss of weight) are as high as 342°C for $\text{Ir}(\text{tntpiq})_2(\text{pop})$ and 377°C for $\text{Ir}(\text{tntpiq})_2(\text{psp})$, respectively. From the DSC curves in **Fig. 2(b)** it can be seen that the melting points (T_m) of $\text{Ir}(\text{tntpiq})_2(\text{pop})$ and $\text{Ir}(\text{tntpiq})_2(\text{psp})$ are as high as 350°C and 338°C , respectively. Both complexes can be vacuum evaporated easily without decomposition, suggesting that both complexes have the potential for use in OLEDs.

3.2. Electrochemical properties and theoretical calculation

The frontier molecular orbitals (FMOs), especially the highest occupied molecular orbital (HOMO) and lowest unoccupied molecular orbital (LUMO) energy levels of the dopants are pretty crucial to the device structure design. Therefore, aiming to measure energy levels of the HOMO/LUMO, the electrochemistry measurements by cyclic voltammetry (CV) were adopted with ferrocene as the internal standard in CH_3CN (**Fig. 3**). The HOMO level was obtained via the oxidation potential and then the LUMO level was calculated by the HOMO and the band gap observed from UV–vis absorption spectra. During the progress of anodic oxidation, an obvious oxide peak can be observed for both complexes with the oxidation potential of 0.99 and 1.04 V, which can be ascribed to the metal-centered Ir(III)/Ir(IV) oxide couple, consistent with the cyclometalated Ir(III) system reported [47]. The cyclic voltammograms of complexes $\text{Ir}(\text{tntpiq})_2(\text{pop})$ and $\text{Ir}(\text{tntpiq})_2(\text{psp})$ show strong oxidation peaks, while the reduction peaks are not obvious,

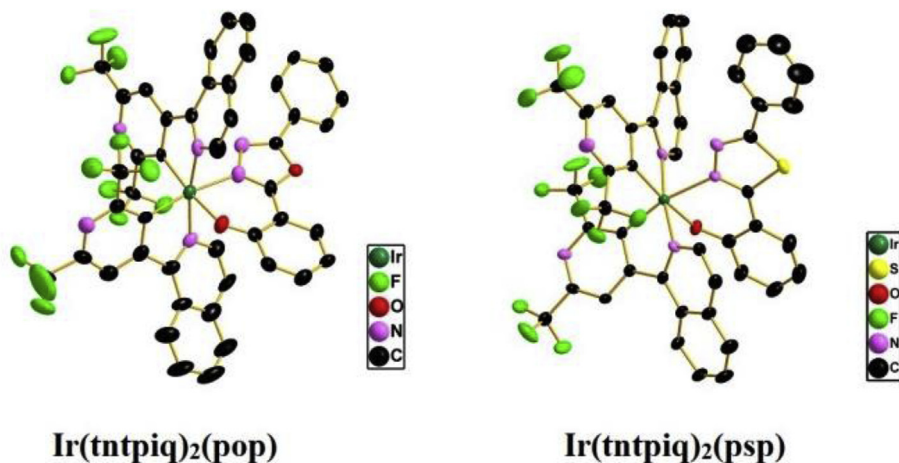


Fig. 1. The crystal diagrams of **Ir(tntpiq)₂(pop)** (CCDC No.1826720) and **Ir(tntpiq)₂(ppy)** (CCDC No. 1826721) shown at 30% probability level. The hydrogen atoms are omitted for clarity.

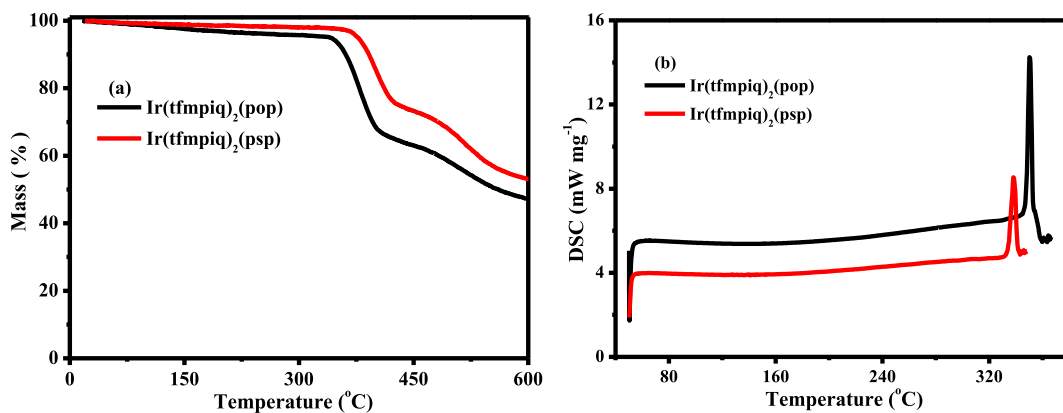


Fig. 2. The TGA (a) and DSC (b) curves of **Ir(tfmpiq)₂(pop)** and **Ir(tfmpiq)₂(ppy)** complexes.

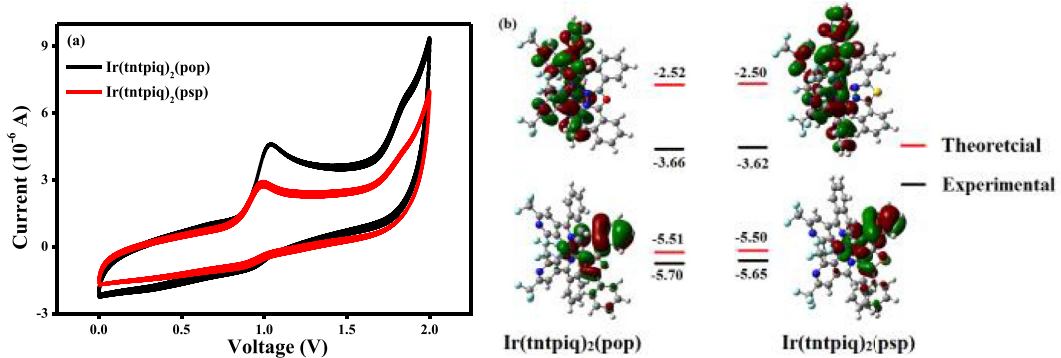


Fig. 3. (a) The cyclic voltammogram curves and (b) contour plots of **Ir(tntpiq)₂(pop)** and **Ir(tntpiq)₂(ppy)**.

demonstrating that the redox process of the complexes **Ir(tntpiq)₂(pop)** and **Ir(tntpiq)₂(ppy)** is not completely reversible, which is also observed in our former publication for Ir(III) complexes with ppy ancillary ligand [44] and other related Ir(III) complexes containing oxadiazole units [48–51]. By comparison between two complexes, the **Ir(tntpiq)₂(ppy)** exhibits a lower oxidation potential (0.99 V) and HOMO/LUMO energy levels are -5.65/-3.62 eV. The oxidation potential of **Ir(tntpiq)₂(pop)** increases to 1.04 V and the HOMO/LUMO energy levels are -5.70/-3.66 eV.

In order to gain insights into the electronic state and the orbital distribution, the density functional theory (DFT) calculations [52] for both Ir(III) complexes were conducted employing Gaussian 09 software with B3LYP function [53]. Plots of the HOMO/LUMO and the molecular orbital energy levels are presented in Fig. 3(b). The basis set used for C, H, N, O and F atoms was 6-31G(d, p) while the LanL2DZ basis set was employed for iridium atoms [54,55]. The solvent effect of CH_2Cl_2 was taken into consideration using conductor like polarizable continuum model (C-PCM). It can be

observed from the theoretical calculation that nearly all LUMOs are on tntpiq ligands (94.80%/93.84%), and rarely situated on iridium atom (3.25%/3.33%) and ancillary ligand (1.96%/2.83%). While HOMOs almost situated on ancillary ligands (80.44%/78.99%), and rarely situated on iridium atom (13.59%/14.59%) and tntpiq ligand (5.97%/6.42%). The rising compositions of HOMOs on the ancillary ligands suggest the photophysical properties of the complexes can be controlled by the modification on the 1,3,4-oxadiazole/1,3,4-thiadiazole derivatives.

3.3. Photophysical property

The UV-vis absorption and photoluminescence spectra of the complexes **Ir(tntpiq)₂(pop)** and **Ir(tntpiq)₂(psp)** in CH₂Cl₂ (5×10^{-5} M) are shown in Fig. 4. The broad and intensive absorption bands below 300 nm are due to the spin-allowed intraligand ¹LC ($\pi-\pi^*$) transition of tntpiq and pop/psp ligands. The weak absorption lasting to 550 nm can be assigned to spin-allowed metal-ligand charge transfer band (¹MLCT) and spin forbidden ³MLCT transition bands caused by the large spin orbital coupling (SOC) which was introduced by Ir(III) center indicating an efficient spin-orbit coupling that is prerequisite for phosphorescent emission. Excited by 397 nm, the strongest emissions peak at 585 and 590 nm in CH₂Cl₂, produced by the electronic transition between the lowest triplet excited state and the ground state, which makes **Ir(tntpiq)₂(pop)** and **Ir(tntpiq)₂(psp)** orange red phosphors. Similar with our former research [44], the psp ancillary ligand resulted the emission red-shift. The emissions in the scope of lower energy around 625 nm may generate by the overlapping vibrational satellites [56]. From Fig. S1(a) (Supporting Information) it can be observed that the PL spectra of two complexes in one popular used host 26DCzPpy (2,6-bis(3-(carbazol-9-yl)pyridin-4-yl)pyridine) are similar with that in CH₂Cl₂ solutions, suggesting the energy transfer between host and dopants. From Fig. S1(b) and Table 1, it can be seen that the PL spectra of **Ir(tntpiq)₂(pop)** and **Ir(tntpiq)₂(psp)** at 77 K remain almost the same. In general, the emission bands from the MLCT states are broad and featureless, whereas a highly structured emission band mainly originates from the ³ $\pi-\pi^*$ state. Accordingly, the emission of **Ir(tntpiq)₂(pop)** and **Ir(tntpiq)₂(psp)** is mainly generated from MLCT states. This indicates that the MLCT characters involved in the emitting T₁ states of different complexes are various but significant, since a dominant MLCT character in T₁ usually leads to large inhomogeneity and low-energy lying metal-ligand vibrational satellites, smearing out the spectrum below the electronic original emission.

Furthermore, the complexes show different quantum efficiencies as 0.41 and 0.59 for **Ir(tntpiq)₂(pop)** and **Ir(tntpiq)₂(psp)**, respectively [57,58]. The differences of the absorption and emission

profiles between **Ir(tntpiq)₂(pop)** and **Ir(tntpiq)₂(psp)** suggest that the ancillary ligand variation has effects on their excited state energy. The phosphorescence lifetime (τ) is the crucial factor that determines the rate of triplet-triplet annihilation in OLEDs. Longer τ values usually cause greater triplet-triplet annihilation. The lifetimes of the complexes are in the range of microseconds (0.95 and 1.08 μ s in CH₂Cl₂ solution, 1.35 and 1.40 μ s in 26DCzPpy, respectively) at room temperature (Fig. S2 and Table 1) and are indicative of the phosphorescent origin for the excited states in each case.

3.4. Electron mobility

According to previous studies, an excellent electron mobility of emitters could benefit electron transport and improve the device performances [25,59]. To determine the electron mobility of two complexes, the transient electroluminescence (TEL) measurement was carried out via the devices with a structure of ITO (indium-tin-oxide)/TAPC (1,1-bis[4-[N,N-di(p-tolyl)amino]pyridin-4-yl]cyclohexane, 50 nm)/Ir(III) complexes (60 nm)/LiF (1 nm)/Al (100 nm). The Ir(III) complexes act as not only the emissive layer (EML) but also electron-transport layer. The experimental results (Fig. 5, Fig. S1) indicated that the electron mobility values of **Ir(tntpiq)₂(pop)** and **Ir(tntpiq)₂(psp)** are $7.20\text{--}7.84 \times 10^{-6}$ cm² V⁻¹ s⁻¹ and $7.56\text{--}8.00 \times 10^{-6}$ cm² V⁻¹ s⁻¹, respectively, under the electric field from 1040 (V cm⁻¹)^{1/2} to 1300 (V cm⁻¹)^{1/2}, higher than of the electron transport material Alq₃ (tris-(8-hydroxyquinoline) aluminium, $4.74\text{--}4.87 \times 10^{-6}$ cm² V⁻¹ s⁻¹) [60]. Additionally, the electron mobility of **Ir(tntpiq)₂(psp)** is a little better than that of **Ir(tntpiq)₂(pop)**. These results are exactly fitting our design intent to improve the electron transport ability of the emitter. The good electron transport ability of **Ir(tntpiq)₂(pop)** and **Ir(tntpiq)₂(psp)** will reinforce the recombination chance of electrons and holes, so that their devices may have good performances.

3.5. OLEDs performance

To confirm our assumption, we researched the single emitting layer (EML) devices **G1** and **G2** using **Ir(tntpiq)₂(pop)** and **Ir(tntpiq)₂(psp)** emitters, respectively, with a structure of ITO/MoO₃ (molybdenum oxide, 3 nm)/TAPC (30 nm)/Ir(III) complexes (x wt%): 26DCzPpy (2,6-bis(3-(carbazol-9-yl)pyridin-4-yl)pyridine, 10 nm)/TmPyPB (1,3,5-tri(*m*-pyrid-3-yl-pyridin-4-yl)benzene, 40 nm)/LiF (1 nm)/Al (100 nm) (Fig. 6). MoO₃ and LiF served as hole- and electron-injecting interface modified materials, respectively. TAPC owning high hole mobility (1×10^{-2} cm² V⁻¹ s⁻¹) and high-lying LUMO level (-2.0 eV) was used as hole transport/electron block layer (HTL/EBL), while TmPyPB with high electron mobility (1×10^{-3} cm² V⁻¹ s⁻¹) and low-lying HOMO level (-6.7 eV) was

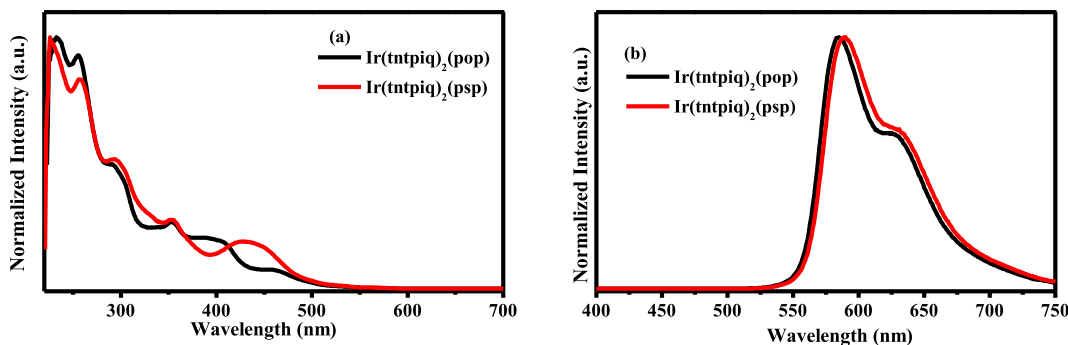


Fig. 4. (a) The UV-vis absorption and (b) emission spectra of **Ir(tntpiq)₂(pop)** and **Ir(tntpiq)₂(psp)** complexes in degassed CH₂Cl₂ solutions (5.0×10^{-5} mol L⁻¹) at room temperature.

Table 1Physical properties of **Ir(tntpiq)₂(pop)** and **Ir(tntpiq)₂(psp)** complexes.

Complex	T_d ^[a]	$\lambda_{abs}^{[b]}$	$\lambda_{em}^{[c]}$		$\phi^{[d]}$	τ^e (μ s)	CIE (x,y)	HOMO/LUMO ^[f]
			298 K	77 K				
Ir(tntpiq)₂(pop)	342	235/255/291/353/380	585	588/639	0.41	0.95	0.558,0.406	-5.70/-3.66
Ir(tntpiq)₂(psp)	377	226/256/294/352/427	590	591/642	0.59	1.08	0.580,0.401	-5.65/-3.62

[a] T_d : decomposition temperature. [b][e] Measured in degassed CH_2Cl_2 solution at a concentration of 5×10^{-5} mol L⁻¹ at room temperature. [c] Measured in degassed CH_2Cl_2 solution at a concentration of 5×10^{-5} mol L⁻¹ at 298 K and 77 K, respectively. [d] Measured in degassed CH_2Cl_2 solution at a concentration of 5×10^{-5} mol L⁻¹ at room temperature emission relative to $\text{Ir}(\text{ppy})_3$ ($\phi = 0.4$). [f] From the onset of oxidation potentials of the cyclovoltammetry (CV) diagram using ferrocene as the internal standard and the optical band gap from the absorption spectra in degassed solution (CH_3CN).

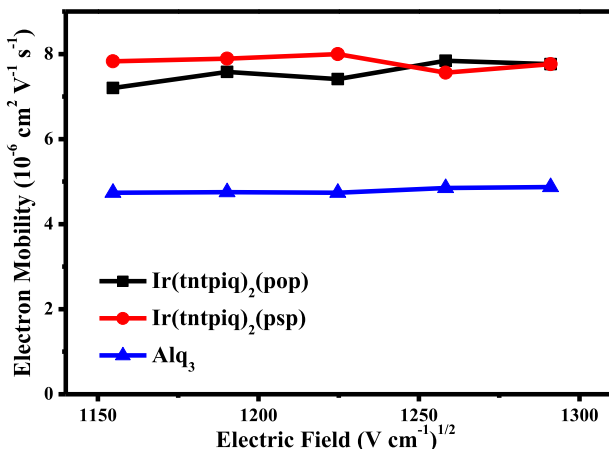


Fig. 5. Electric field dependence of charge electron mobility in the thin films of **Ir(tntpiq)₂(pop)**, **Ir(tntpiq)₂(psp)** and Alq_3 .

used as electron transport/hole block layer (ETL/HBL). Ambipolar material 26DCzPPy was chosen as the host because its' nearly equal electron mobility (μ_e) and hole mobility (μ_h) values ($1-8 \times 10^{-5}$ $\text{cm}^2 \text{ V}^{-1} \text{ s}^{-1}$ at an electric field between 6.0×10^5 and $1.0 \times 10^6 \text{ V cm}^{-1}$), which benefits the electron-hole balance in the EML [61–63]. The optimal device performances are achieved at doping level of 2 wt% for **Ir(tntpiq)₂(pop)** and **Ir(tntpiq)₂(psp)** complexes.

The EL spectra, luminance-voltage-current density (L - V - J) curves, current efficiency-luminance (η_c - L) curves, power efficiency-luminance (η_p - L) curves for **G1** and **G2** are shown in Fig. 7, and the crucial EL data are summarized in Table 2. The peaks of EL emission are 585 and 587 nm for **G1** and **G2**, respectively. The

emission spectra are almost invariant of the current density and there is no dependence on concentration. From Fig. 7(a) it can be seen that the EL spectra are almost identical to the PL spectra of the complexes, suggesting that the devices' EL emissions come from the triplet excited states of the phosphors. Apart from the characteristic emissions of Ir(III) complexes, both devices also displayed weak emissions range from 350 nm to 500 nm, which originate from the host 26DCzPPy attributed to the accumulation of holes and electrons within the EML and few holes/electrons would recombine on 26DCzPPy molecules. And the Commission Internationale de l'Eclairage (CIE) color coordinates of **G1** and **G2** are (0.558, 0.406) and (0.580, 0.401), respectively.

For the device **G1**, a maximum luminance (L_{max}) of 31 413 cd m⁻², a maximum current efficiency ($\eta_{c,max}$) of 24.9 cd A⁻¹ (5.6 V) with a maximum external quantum efficiency (EQE_{max}) of 11.9%, a maximum power efficiency ($\eta_{p,max}$) of 14.3 lm W⁻¹ (5.4 V) are obtained. While the device **G2** displays similar EL performances with a $\eta_{c,max}$ of 24.3 cd A⁻¹ (5.8 V), an EQE_{max} of 11.6%, a $\eta_{p,max}$ of 15.2 lm W⁻¹ (5.0 V) and a L_{max} of 27 348 cd m⁻² at 13.9 V. It is noteworthy that both devices show very mild efficiency roll-off. For device **G1**, the η_c and EQE values at the practical brightness of 100 cd m⁻² are 21.9 cd A⁻¹ and 10.5%, respectively. Even at the high luminance of 1000 cd m⁻² these values are still kept at 21.7 cd A⁻¹ and 10.3%, respectively. Device **G2** even exhibits lower efficiency roll-off with these values as 24.1 cd A⁻¹ and 11.5% at 100 cd m⁻² and 23.1 cd A⁻¹ and 11.0% at 1000 cd m⁻², respectively.

The introduction of 1,3,4-oxadiazole and 1,3,4-thiadiazole derivatives in the ancillary ligand not only increased the electron mobility of the Ir(III) complexes, but also enhanced their PL quantum efficiencies, which will benefit the OLED performances. The good electron mobility of the phosphorescent emitter would facilitate the injection and transport of electrons, which would broaden the recombination zone, balance the distribution of holes

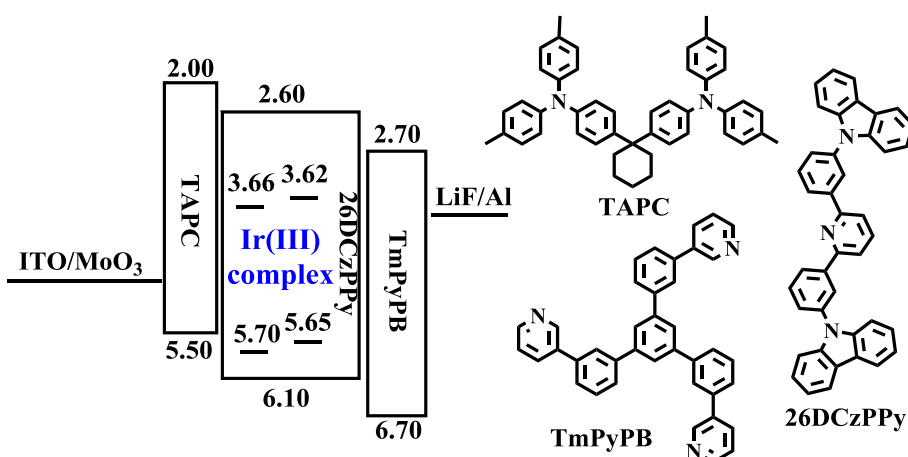


Fig. 6. Energy level diagram of HOMO and LUMO levels (relative to vacuum level) for materials investigated in this work and their molecular structures.

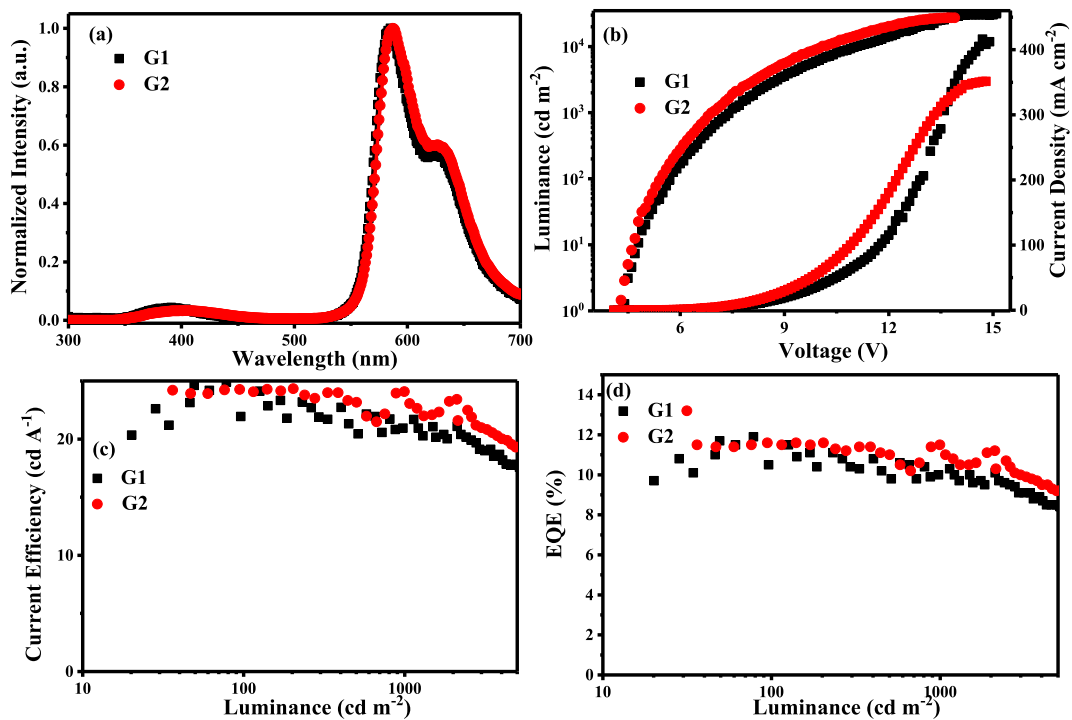


Fig. 7. Characteristics of devices **G1** and **G2**: (a) electroluminescence spectra (8 V); (b) luminance – voltage – current density (L – V – J) curves; (c) current efficiency – luminance (η_c – L) curves; (d) power efficiency – luminance (η_p – L) curves.

Table 2
EL performances of **G1** and **G2**.

device	$V_{\text{turn-on}}^{\text{a}}$ (V)	L_{\max}^{b} (cd m $^{-2}$)	$\eta_{c,\max}^{\text{c}}$ (cd A $^{-1}$)	$\eta_{c,L100}^{\text{d}}$ (cd A $^{-1}$)	$\eta_{c,L1000}^{\text{e}}$ (cd A $^{-1}$)	$\text{EQE}_{\max}^{\text{f}}$ (%)	$\text{EQE}_{L100}^{\text{g}}$ (%)	$\text{EQE}_{L1000}^{\text{h}}$ (%)	$\eta_{p,\max}^{\text{i}}$ (lm W $^{-1}$)
G1	4.3	31413	24.9	21.9	21.7	11.9	10.5	10.3	14.3
G2	4.2	27348	24.3	24.1	23.1	11.6	11.5	11.0	15.2

^a $V_{\text{turn-on}}$: turn-on voltage recorded at a luminance of 1 cd m $^{-2}$.

^b L_{\max} : maximum luminance.

^c $\eta_{c,\max}$: maximum current efficiency.

^d $\eta_{c,L100}$: current efficiency at 100 cd m $^{-2}$.

^e $\eta_{c,L1000}$: current efficiency at 1000 cd m $^{-2}$.

^f EQE_{\max} : maximum external quantum efficiency.

^g EQE_{L100} : external quantum efficiency at 100 cd m $^{-2}$.

^h EQE_{L1000} : external quantum efficiency at 1000 cd m $^{-2}$.

ⁱ $\eta_{p,\max}$: maximum power efficiency.

and electrons, particularly at a high doping concentration, leading to the suppressed TTA and TPA effects. The high electron mobility of complexes would lead to a good-balanced charge carrier transport and efficient recombination, which is agree with the design intention.

4. Conclusion

In conclusion, two bis-cyclometalated Ir(III) complexes (**Ir(tnt-piq)₂(pop)** and **Ir(tntpqi)₂(psp)**) with 2-(5-pyridin-4-yl)-1,3,4-oxadiazol-2-yl)phenol, 2-(5-pyridin-4-yl)-1,3,4-thiadiazol-2-yl phenol as ancillary ligands and 1-(3,5-bis(trifluoromethyl)pyridin-4-yl)isoquinoline as the main ligand were investigated. Due to the trifluoromethyl substituted nitrogen heterocyclic structure of the main ligand and 1,3,4-oxadiazole/1,3,4-thiadiazol moieties in the ancillary ligands, both complexes emit orange red phosphorescence with high quantum efficiency and good electron mobility. The good electron mobility would improve a good-balanced charge carrier transport and efficient recombination of both complexes, resulting in an EQE_{\max} of 11.6% with very mild efficiency roll-off.

The EQE values of 11.5% and 11.0% still can be obtained at the practical luminance of 100 cd m $^{-2}$ and 1000 cd m $^{-2}$, respectively.

Acknowledgements

This work was supported by the National Natural Science Foundation of China (51773088), the Natural Science Foundation of Jiangsu Province (BY2016075-02) and the Fundamental Research Funds for the Central Universities (020514380131).

Appendix A. Supplementary data

Supplementary data to this article can be found online at <https://doi.org/10.1016/j.jorgchem.2018.09.008>.

References

- [1] S. Lamansky, P. Djurovich, D. Murphy, F. Abdel-Razzaq, H.E. Lee, C. Adachi, P.E. Burrows, S.R. Forrest, M.E. Thompson, Highly phosphorescent bis-cyclometalated iridium complexes: synthesis, photophysical characterization, and use in organic light emitting diodes, *J. Am. Chem. Soc.* 123 (2001)

- 4304–4312.
- [2] J.J. Kim, Y. You, Y.S. Park, J.J. Kim, S.Y. Park, Dendritic Ir(III) complexes functionalized with triphenylsilylphenyl groups: synthesis, DFT calculation and comprehensive structure-property correlation, *J. Mater. Chem.* 19 (2009) 8347–8359.
- [3] S.M. Chen, G.P. Tan, W.Y. Wong, H.S. Kwok, White organic light-emitting diodes with evenly separated red, green, and blue colors for efficiency/color-rendition trade-off optimization, *Adv. Funct. Mater.* 21 (2011) 3785–3793.
- [4] J.M. Fernández-Hernández, C.H. Yang, J.I. Beltrán, V. Lemaur, F. Polo, R. Frohlich, J. Cornil, L. De Cola, Control of the mutual arrangement of cyclometalated ligands in cationic iridium(III) complexes: synthesis, spectroscopy, and electroluminescence of the different isomers, *J. Am. Chem. Soc.* 133 (2011) 10543–10558.
- [5] K.Y. Lu, H.H. Chou, C.H. Hsieh, Y.H. Ou Yang, H.R. Tsai, H.Y. Tsai, L.C. Hsu, C.Y. Chen, I.C. Chen, C.H. Cheng, Wide-range color tuning of iridium biscarbene complexes from blue to red by different N,N ligands: an alternative route for adjusting the emission colors, *Adv. Mater.* 23 (2011) 4933–4937.
- [6] S. Lee, S.O. Kim, H. Shin, H.J. Yun, K. Yang, S.K. Kwon, J.J. Kim, Y.H. Kim, Deep-blue phosphorescence from perfluoro carbonyl-substituted iridium complexes, *J. Am. Chem. Soc.* 135 (2013) 14321–14328.
- [7] X.L. Yang, N. Sun, J.S. Dang, Z. Huang, C.L. Yao, X.B. Xu, C.L. Ho, G.J. Zhou, D.G. Ma, X. Zhao, W.Y. Wong, Versatile phosphorescent color tuning of highly efficient borylated iridium(III) cyclometalates by manipulating the electron-accepting capacity of the dimesitylboron group, *J. Mater. Chem. C* 1 (2013) 3317–3326.
- [8] H. Sasabe, H. Nakaniishi, Y. Watanabe, S. Yano, M. Hirasawa, Y.J. Pu, J. Kido, Extremely low operating voltage green phosphorescent organic light-emitting devices, *Adv. Funct. Mater.* 23 (2013) 5550–5555.
- [9] H.-H. Chou, Y.-K. Li, Y.-H. Chen, C.-C. Chang, C.-Y. Liao, C.-H. Cheng, New iridium dopants for white phosphorescent devices: enhancement of efficiency and color stability by an energy-harvesting layer, *ACS Appl. Mater. Interfaces* 5 (2013) 6168–6175.
- [10] H. Cao, H. Sun, Y. Yin, X. Wen, G. Shan, Z. Su, R.N. Zhong, W. Xie, P. Li, D. Zhu, Iridium(III) complexes adopting 1,2-diphenyl-1H-benzimidazole ligands for highly efficient organic light-emitting diodes with low efficiency roll-off and non-doped feature, *J. Mater. Chem. C* 2 (2014) 2150–2159.
- [11] A. Graf, P. Liehm, C. Murawski, S. Hofmann, K. Leo, M.C. Gather, Correlating the transition dipole moment orientation of phosphorescent emitter molecules in OLEDs with basic material properties, *J. Mater. Chem. C* 2 (2014) 10298–10304.
- [12] X. Xu, X. Yang, J. Dang, G. Zhou, Y. Wu, H. Li, W.-Y. Wong, Trifunctional Ir^{III}ppy-type asymmetric phosphorescent emitters with ambipolar features for highly efficient electroluminescent devices, *Chem. Commun.* 50 (2014) 2473–2476.
- [13] X. Yang, G. Zhou, W.Y. Wong, Recent design tactics for high performance white polymer light-emitting diodes, *J. Mater. Chem. C* 2 (2014) 1760–1788.
- [14] W.-Y. Wong, C.-L. Ho, Functional metallophosphors for effective charge carrier injection/transport: new robust OLED materials with emerging applications, *J. Mater. Chem.* 19 (2009) 4457–4482.
- [15] W.-Y. Wong, C.-L. Ho, Heavy metal organometallic electrophosphors derived from multi-component chromophores, *Coord. Chem. Rev.* 253 (2009) 1709–1758.
- [16] G.J. Zhou, W.-Y. Wong, S. Suo, Recent progress and current challenges in phosphorescent white organic light-emitting diodes (WOLEDs), *J. Photochem. Photobiol. C Photocomp. Rev.* 11 (2010) 133–156.
- [17] G.J. Zhou, W.-Y. Wong, X.L. Yang, New design tactics in OLEDs using functionalized 2-phenylpyridine-type cyclometalates of iridium(III) and platinum(II), *Chem. Asian J.* 6 (2011) 1706–1727.
- [18] C.-L. Ho, W.-Y. Wong, Small-molecular blue phosphorescent dyes for organic light-emitting devices, *New J. Chem.* 37 (2013) 1665–1683.
- [19] C.-L. Ho, W.-Y. Wong, Charge and energy transfers in functional metallophosphors and metallopolyenes, *Coord. Chem. Rev.* 257 (2013) 1614–1649.
- [20] L. Ying, C.-L. Ho, H.B. Wu, Y. Cao, W.-Y. Wong, White polymer light-emitting devices for solid-state lighting: materials, devices, and recent progress, *Adv. Mater.* 26 (2014) 2459–2473.
- [21] C.-L. Ho, H. Li, W.-Y. Wong, Red to near-infrared organometallic phosphorescent dyes for OLED applications, *J. Organomet. Chem.* 751 (2014) 261–285.
- [22] X.L. Yang, G.J. Zhou, W.-Y. Wong, Functionalization of phosphorescent emitters and their host materials by main-group elements for phosphorescent organic light-emitting devices, *Chem. Soc. Rev.* 44 (2015) 8484–8575.
- [23] X.B. Xu, X.L. Yang, J. Zhao, G.J. Zhou, W.-Y. Wong, Recent advances in solution-processable dendrimers for highly efficient phosphorescent organic light-emitting diodes (PhOLEDs), *Asian J. Org. Chem.* 4 (2015) 394–429.
- [24] G. Sarada, J. Yoon, W. Cho, M. Cho, D.W. Cho, S.O. Kang, Y. Nam, J.Y. Lee, S.-H. Jin, Substituent position engineering of diphenylquinoline-based Ir(III) complexes for efficient orange and white PhOLEDs with high color stability/low efficiency roll-off using a solution-processed emission layer, *J. Mater. Chem. C* 4 (2016) 113–120.
- [25] G. Sarada, J. Yoon, W. Cho, M. Cho, D.W. Cho, S.O. Kang, Y. Nam, J.Y. Lee, S.-H. Jin, Substituent position engineering of diphenylquinoline-based Ir(III) complexes for efficient orange and white PhOLEDs with high color stability/low efficiency roll-off using a solution-processed emission layer, *J. Mater. Chem. C* 4 (2016) 113–120.
- [26] J.P. Duan, P.-P. Sun, C.-H. Cheng, New iridium complexes as highly efficient orange-red emitters in organic light-emitting diodes, *Adv. Mater.* 15 (2003) 224–228.
- [27] D. Liu, H. Ren, L. Deng, T. Zhang, Synthesis and electrophosphorescence of iridium complexes containing benzothiazole-based ligands, *ACS Appl. Mater. Interfaces* 5 (2013) 4937–4944.
- [28] Z. Yan, Y. Wang, J. Ding, Y. Wang, L. Wang, Highly efficient phosphorescent furo[3,2-c]pyridine based iridium complexes with tunable emission colors over the whole visible range, *ACS Appl. Mater. Interfaces* 10 (2018) 1888–1896.
- [29] W.S. Jeon, T.J. Park, S.Y. Kim, R. Pode, J. Jang, J.H. Kwon, Low roll-off efficiency green phosphorescent organic light-emitting devices with simple double emissive layer structure, *Appl. Phys. Lett.* 93 (2008), 063303.
- [30] Y.T. Tao, C.L. Yang, J.G. Qin, Organic host materials for phosphorescent organic light-emitting diodes, *Chem. Soc. Rev.* 40 (2011) 2943–2970.
- [31] C.-L. Ho, W.-Y. Wong, Q. Wang, D.G. Ma, L.X. Wang, Z.Y. Lin, A multifunctional iridium-carbazolyl orange phosphor for high-performance two-element WOLED exploiting exciton-managed fluorescence/phosphorescence, *Adv. Funct. Mater.* 18 (2008) 928–937.
- [32] X.J. Liu, B. Yao, Z.L. Zhang, X.F. Zhao, B.H. Zhang, W.-Y. Wong, Y.X. Cheng, Z.Y. Xie, Power-efficient solution-processed red organic light-emitting diodes based on an complex host and a novel phosphorescent iridium complex, *J. Mater. Chem. C* 4 (2016) 5787–5794.
- [33] X.J. Liu, B. Yao, H.L. Wang, B.H. Zhang, X.D. Lin, X.F. Zha, Y.X. Cheng, Z.Y. Xie, W.-Y. Wong, Efficient solution-processed yellow/orange phosphorescent OLEDs based on heteroleptic Ir(III) complexes with 2-(9,9-diethylfluorene-2-yl)pyridine main ligand and various ancillary ligands, *Org. Electron.* 54 (2018) 197–203.
- [34] Q.L. Xu, X. Liang, S. Zhang, Y.M. Jing, X. Liu, G.Z. Lu, Y.X. Zheng, J.L. Zuo, Efficient OLEDs with low efficiency roll-off using iridium complexes possessing good electron mobility, *J. Mater. Chem. C* 3 (2015) 3694–3701.
- [35] Y.M. Jing, Y. Zhao, Y.X. Zheng, Photoluminescence and electroluminescence of iridium(III) complexes with 2',6'-bis(trifluoromethyl)-2,4'-bipyridine and 1,3,4-oxadiazole/1,3,4-thiadiazole derivatives ligands, *Dalton Trans.* 46 (2017) 845–853.
- [36] H.B. Han, R.Z. Cui, Y.M. Jing, G.Z. Lu, Y.X. Zheng, L. Zhou, J.L. Zuo, H. Zhang, Highly efficient red electroluminescence of iridium complexes with 1-(2,6-bis(trifluoromethyl)pyridin-4-yl)isoquinoline and 4-(2,6-bis(trifluoromethyl)pyridin-4-yl)quinazoline main ligands, *J. Mater. Chem. C* 5 (2017) 8150–8159.
- [37] H.B. Han, R.Z. Cui, G.Z. Lu, Z.G. Wu, Y.X. Zheng, L. Zhou, H. Zhang, Efficient orange-red electroluminescence of iridium complexes with 1-(2,6-bis(trifluoromethyl)pyridin-4-yl) isoquinoline and 4-(2,6-bis(trifluoromethyl)pyridin-4-yl)quinazoline ligands, *Dalton Trans.* 46 (2017) 14916–14925.
- [38] Z. He, W.Y. Wong, X. Yu, H.S. Kwok, Z. Lin, Phosphorescent platinum(II) complexes derived from multifunctional chromophores: synthesis, structures, photophysics, and electroluminescence, *Inorg. Chem.* 45 (2006) 10922–10937.
- [39] W.Y. Wong, Z. He, S.K. So, K.L. Tong, Z. Lin, A multifunctional platinum-based triplet emitter for OLED applications, *Organometallics* 24 (2005) 4079–4082.
- [40] H.Y. Li, T.Y. Li, M.Y. Teng, Q.L. Xu, S. Zhang, Y.M. Jin, X. Liu, Y.X. Zheng, J.L. Zuo, Syntheses, photoluminescence and electroluminescence of four heteroleptic iridium complexes with 2-(5-phenyl-1,3,4-oxadiazol-2-yl)-phenol derivatives as ancillary ligands, *J. Mater. Chem. C* 2 (2014) 1116–1124.
- [41] SAINT-plus, Version 6.02, Bruker Analytical X-ray System, Madison, WI, 1999.
- [42] G.M. Sheldrick, SADABS An Empirical Absorption Correction Program, Bruker Analytical X-ray Systems, Madison, WI, 1996.
- [43] G.M. Sheldrick, SHELXTL-2014, Universität of Göttingen, Göttingen, Germany, 2014.
- [44] X. Liu, S. Zhang, Y.M. Jin, G.Z. Lu, L. Jiang, X. Liang, Q.L. Xu, Y.X. Zheng, Syntheses, crystal structure and photophysical property of iridium complexes with 1,3,4-oxadiazole and 1,3,4-thiadiazole derivatives as ancillary ligands, *J. Organomet. Chem.* 785 (2015) 11–18.
- [45] H.Y. Li, T.Y. Li, Q. Liu, Q.L. Xu, C.C. Wang, S. Zhang, C. Lin, W. Huang, Y.X. Zheng, X.Q. Wang, Synthesis, photoluminescence and computational study of rhodium(I) diimine complexes with [1,3,4]oxadiazole substituted 2,2'-bipyridine ligands, *J. Organomet. Chem.* 743 (2013) 37–43.
- [46] G.Z. Lu, Y.M. Jing, H.B. Han, Y.L. Fang, Y.X. Zheng, Efficient electroluminescence of two heteroleptic platinum complexes with 2-(5-phenyl-1,3,4-oxadiazol-2-yl)-phenol as ancillary ligand, *Organometallics* 36 (2017) 448–454.
- [47] S. Bettington, M. Tavasli, M.R. Bryce, A. Beeby, H. Al-Attar, A.P. Monkman, Tris-cyclometalated iridium(III) complexes of carbazole(fluorenyl)pyridine ligands: synthesis, redox and photophysical properties, and electro-phosphorescent light-emitting diodes, *Chem. Eur. J.* 13 (2007) 1423–1431.
- [48] L.Q. Chen, H. You, C.L. Yang, D.G. Ma, J.G. Qin, Novel, highly efficient blue-emitting heteroleptic iridium(III) complexes based on fluorinated 1,3,4-oxadiazole: tuning to blue by dithiolate ancillary ligands, *Chem. Commun.* (2007) 1352–1354.
- [49] Z. Xu, Y. Li, X. Ma, X. Gao, H. Tian, Synthesis and properties of iridium complexes based 1,3,4-oxadiazoles derivatives, *Tetrahedron* 64 (2008) 1860–1867.
- [50] Y.H. Zheng, A.S. Batsanov, M.R. Bryce, Unusual dinuclear and mononuclear cyclometalated iridium complexes of 2,5-diaryl-1,3,4-oxadiazole derivatives, *Inorg. Chem.* 50 (2011) 3354–3362.
- [51] Q.L. Xu, H.Y. Li, C.C. Wang, S. Zhang, T.Y. Li, Y.M. Jing, Y.X. Zheng, W. Huang, J.L. Zuo, X.Z. You, Synthesis, structure, photophysical and electrochemical

- properties of series of new *fac*-triscyclometallated iridium complexes with carbazole or oxadiazole moieties, *Inorg. Chim. Acta.* 391 (2012) 50–57.
- [52] E. Runge, E.K.U. Gross, Density-functional theory for time-dependent systems, *Phys. Rev. Lett.* 52 (1984) 997.
- [53] M.J. Frisch, G.W. Trucks, H.B. Schlegel, G.E. Scuseria, M.A. Robb, J.R. Cheeseman, G. Scalmani, V. Barone, B. Mennucci, G.A. Petersson, H. Nakatsuji, M. Caricato, X. Li, H.P. Hratchian, A.F. Izmaylov, J. Bloino, G. Zheng, J.L. Sonnenberg, M. Hada, M. Ehara, K. Toyota, R. Fukuda, J. Hasegawa, M. Ishida, T. Nakajima, Y. Honda, O. Kitao, H. Nakai, T. Vreven, J.A. Montgomery Jr., J.E. Peralta, F. Ogliaro, M. Bearpark, J.J. Heyd, E. Brothers, K.N. Kudin, V.N. Staroverov, R. Kobayashi, J. Normand, K. Raghavachari, A. Rendell, J.C. Burant, S.S. Iyengar, J. Tomasi, M. Cossi, N. Rega, J.M. Millam, M. Klene, J.E. Knox, J.B. Cross, V. Bakken, C. Adamo, J. Jaramillo, R. Gomperts, R.E. Stratmann, O. Yazyev, A.J. Austin, R. Cammi, C. Pomelli, J.W. Ochterski, R.L. Martin, K. Morokuma, V.G. Zakrzewski, G.A. Voth, P. Salvador, J.J. Dannenberg, S. Dapprich, A.D. Daniels, O. Farkas, J.B. Foresman, J.V. Ortiz, J. Cioslowski, D.J. Fox, Gaussian 09, Revision A.01, Gaussian, Inc., Wallingford, CT, 2009.
- [54] W.R. Wadt, P.J. Hay, Ab initio effective core potentials for molecular calculations. Potentials for main group elements Na to Bi, *J. Phys. Chem.* 82 (1985) 284–298.
- [55] P.J. Hay, W.R. Wadt, Ab initio effective core potentials for molecular calculations. Potentials for K to Au including the outermost core orbitals, *J. Chem. Phys.* 82 (1985) 299–310.
- [56] A.F. Rausch, M.E. Thompson, H. Yersin, Matrix effects on the triplet state of the OLED emitter $\text{Ir}(4,6\text{-dFppy})_2(\text{pic})$ (Flrpic): investigations by high-resolution optical spectroscopy, *Inorg. Chem.* 48 (2009) 1928–1937.
- [57] K.A. King, P.J. Spellane, R.J. Watts, Excited-state properties of a triply ortho-metallated iridium(III) complex, *J. Am. Chem. Soc.* 107 (1985) 1431–1432.
- [58] K. Dedeian, P.I. Djurovich, F.O. Garces, G. Carlson, R.J. Watts, A new synthetic route to the preparation of a series of strong photoreducing agents: *fac*-tris-ortho-metallated complexes of iridium(III) with substituted 2-phenyl-pyridines, *Inorg. Chem.* 30 (1991) 1685–1687.
- [59] J. Kalinowski, W. Stämpfli, J. Mezyk, M. Cocchi, D. Virgili, V. Fattori, P. Di Marco, Quenching effects in organic electrophosphorescence, *Phys. Rev. B Condens. Matter* 66 (2002) 235321.
- [60] A.J. Pal, R. Osterbacka, K.M. Kallman, H. Stubb, Transient electroluminescence: mobility and response time in quinque thiophene Langmuir–Blodgett films, *Appl. Phys. Lett.* 71 (1997) 228.
- [61] J. Lee, N. Chopra, S.H. Eom, Y. Zheng, J. Xue, F. So, J. Shi, Effects of triplet energies and transporting properties of Carrier transporting materials on blue phosphorescent organic light emitting devices, *Appl. Phys. Lett.* 93 (2008) 123306.
- [62] S.J. Su, T. Chiba, T. Takeda, J. Kido, Pyridine-containing triphenylbenzene derivatives with high electron mobility for highly efficient phosphorescent OLEDs, *Adv. Mater.* 20 (2008) 2125–2130.
- [63] M. Imai, S. Tokito, Y. Sakamoto, T. Suzuki, Y. Taga, Highly efficient phosphorescence from organic light-emitting devices with an exciton-block layer, *Appl. Phys. Lett.* 79 (2001) 156.